The Gradient Velocity Track Display (GrVTD) Technique for Retrieving Tropical Cyclone Primary Circulation from Aliased Velocities Measured by Single-Doppler Radar

MINGJUN WANG

Key Laboratory for Mesoscale Severe Weather/MOE, and School of Atmospheric Science, Nanjing University, Nanjing, China, and Center for Analysis and Prediction of Storms, University of Oklahoma, Norman, Oklahoma

KUN ZHAO

Key Laboratory for Mesoscale Severe Weather/MOE, and School of Atmospheric Science, Nanjing University, Nanjing, China

WEN-CHAU LEE

National Center for Atmospheric Research, Boulder, Colorado

BEN JONG-DAO JOU

Department of Atmospheric Sciences, National Taiwan University, Taipei, Taiwan

MING XUE

Center for Analysis and Prediction of Storms, and School of Meteorology, University of Oklahoma, Norman, Oklahoma

(Manuscript received 7 December 2011, in final form 22 February 2012)

ABSTRACT

The ground-based velocity track display (GBVTD) technique was developed to estimate the primary circulations of landfalling tropical cyclones (TCs) from single-Doppler radar data. However, GBVTD cannot process aliased Doppler velocities, which are often encountered in intense TCs. This study presents a new gradient velocity track display (GrVTD) algorithm that is essentially immune to the Doppler velocity aliasing. GrVTD applies the concept of gradient velocity–azimuth display (GVAD) to the GBVTD method. A GrVTD-simplex algorithm is also developed to accompany GrVTD as a self-sufficient algorithm suite.

The results from idealized experiments demonstrate that the circulation center and winds retrieved from GrVTD with aliased velocity and GBVTD with dealiased velocity are in good agreement, but GrVTD is more sensitive to random observation errors. GrVTD was applied to Hurricane Charley (2004) where the majority of the Doppler velocities of the inner-core region were aliased. The GrVTD-retrieved circulation pattern and magnitude are nearly identical to those retrieved in GBVTD with manually dealiased velocities. Overall, the performance of GrVTD is comparable but is more sensitive to the data distribution than that of the original GBVTD using dealiased velocity. GrVTD can be used as a preprocessor for dealiasing velocity in TCs before the data are used in GBVTD or other algorithms.

1. Introduction

Tropical cyclones (TCs) have long been recognized as a large cyclonically rotating vortex possessing a dipole Doppler velocity pattern in a plan position indicator (PPI) display, as portrayed in Baynton (1979). Wood and Brown (1992) illustrated that the characteristics of a TC approximated by an idealized Rankine vortex—including its center, radius of maximum wind (RMW), and the maximum wind speed—can be estimated from the location and magnitude of this Doppler velocity dipole. Radial inflow (outflow) near the RMW can be inferred if the aforementioned pattern rotates clockwise (counterclockwise). In their framework, only three pieces

Corresponding author address: Kun Zhao, Key Laboratory of Mesoscale Severe Weather/MOE, School of Atmospheric Sciences, Nanjing University, 22 Hankou Road, Nanjing 210093, China.
E-mail: zhaokun@nju.edu.cn

DOI: 10.1175/JTECH-D-11-00219.1

of information—that is, the location, magnitude, and rotation rate of the Doppler velocity dipole—are used; therefore, only qualitative and limited quantitative TC structure near the RMW can be obtained.

By using all available Doppler velocities in a constant altitude PPI (CAPPI), the velocity track display (VTD) technique (Lee et al. 1994) formulates a more complete mathematical representation between the TC primary circulation and the observed Doppler velocities, enabling the reconstruction of three-dimensional (3D) primary circulations of TCs from data collected by a single airborne Doppler radar. A series of VTD extensions (referred to as the ''VTD family of techniques'')—including extended VTD (EVTD; Roux and Marks 1996), the ground-based VTD (GBVTD; Lee et al. 1999, hereafter LJCD), ground-based extended VTD (GB-EVTD; Roux et al. 2004), extended GBVTD (EGBVTD; Liou et al. 2006), and generalized VTD (GVTD; Jou et al. 2008)—expanded the VTD analysis into multiple flight legs for airborne Doppler radar and multiple ground-based Doppler radars (e.g., Roux and Marks 1996; Lee et al. 2000; Harasti et al. 2004; Liou et al. 2006; Lee and Bell 2007; Zhao et al. 2008). Recently, the GBVTD technique has been incorporated into the Vortex Objective Radar Tracking and Circulation (VORTRAC) software for real-time analysis of TCs at the National Hurricane Center (NHC) of the United States. Despite the tremendous utility of the VTD family of techniques in deducing TC centers and their associated primary circulations, all of the aforementioned algorithms will fail when a significant amount of aliased Doppler velocities exist.[1]

Doppler velocity aliasing occurs when the magnitude of the radial component of the true 3D velocity exceeds the unambiguous (or Nyquist) velocity of a radar V_N given by

$$V_N = \frac{\mathrm{PRF} \times \lambda}{4}, \tag{1}$$

where PRF is the pulse repetition frequency and λ is the wavelength of the radar (Doviak and Zrnic 2006). The measured Doppler velocity V_d is related to the true velocity V_u by

$$V_u = V_d \pm 2nV_N, \tag{2}$$

where the integer n is the number of Nyquist intervals between the true Doppler velocity V_u and the measured velocity V_d satisfying $V_N \geq V_d \geq -V_N$. The purpose of dealiasing (commonly known as ''unfolding'') is to determine the proper value of n for each velocity measurement.

Typical S-band (λ = 10 cm) and C-band (λ = 5 cm) Doppler radars transmitting a PRF = 1000 Hz possess V_N of 25 and 12.5 m s^{-1}, respectively. The wind speeds in the inner-core region of a TC with tropical storm and above intensity exceed 25 m s^{-1}. As a result, velocity aliasing is the norm rather than the exception for most of the operational Doppler radars. For category 3–5 hurricanes (>53 m s^{-1}), multiple folds ($n > 1$) of Doppler velocity will occur for a C-band radar, especially in the inner-core region critical to diagnosing TC intensity. Hence, the VTD family of algorithms requires that the input Doppler velocities are dealiased as a priori. Manual dealiasing using software such as SOLO (Oye et al. 1995) is time consuming and an acceptable option only for post analysis and research, but not for real-time operations. Existing batch/automated dealiasing algorithms (see discussions next) are usually not sufficiently robust (Xu et al. 2011). It is desirable to develop an improved VTD family of algorithms that is immune to velocity aliasing for both research and real-time operational use.

There are two main methods to tackle the aliasing problem: 1) the staggered pulse repetition frequency (PRF) technique (e.g., Doviak and Zrnic 2006) and the multiple PRF technique (Zittel and Wiegman 2005) implemented in selected Weather Surveillance Radar-1988 Doppler (WSR-88D) volume coverage patterns (VCPs), and 2) automated dealiasing algorithms (e.g., Bargen and Brown 1980; Bergen and Albers 1988; and others). For the majority of the Doppler radars in the world, using various dealiasing algorithms remains the only viable option. Velocity dealiasing algorithms typically rely on properly identified velocity folding with a reference velocity and/or continuity with adjacent velocities (Gong et al. 2003). These dealiasing algorithms usually examine the continuity of the Doppler velocities in dimensions ranging from zero (e.g., using environmental wind as a reference; Hennington 1981), one (e.g., either radially or azimuthally; Bargen and Brown 1980), two and/or three (e.g., Miller et al. 1986; Bergen and Albers 1988; Gao and Droegemeier 2004; Jing and Wiener 1993), to four in space and time (e.g., James and Houze 2001). The success of these algorithms more or less relies on properly identifying an absolute velocity reference within the analysis domain, which can be problematic in practice.

A different approach has been developed in recent years for certain wind retrieval algorithms that do not require a reference velocity as a priori or can use aliased Doppler velocity directly. Yamada and Chong (1999)

[1] The VTD family of techniques uses low-order Fourier wavenumber expansion. Hence, they have some immunity to a small amount of random aliased Doppler velocities.

applied velocity–azimuth display (VAD) winds as a constraint to determine the proper number of folds in the data. The gradient VAD (GVAD; Tabary et al. 2001; Gao et al. 2004) uses the azimuthal Doppler velocity gradient rather than the actual Doppler velocity in the VAD framework and therefore does not require dealiasing a priori. Because the azimuthal Doppler velocity gradient is continuous, except for finite locations along a full VAD circle where Doppler velocity crosses V_N (defined as "folding points"), GVAD discards these gradients at the folding points. GVAD can be performed using aliased Doppler velocities directly and can handle Doppler velocity with multiple folds. Since errors are amplified by taking derivatives, GVAD results tend to be more sensitive to noise, poor data quality, and uneven data distributions than the VAD. A series of general dealiasing algorithms based on the VAD and GVAD approaches has been developed primarily for radar data quality control and assimilation purposes and has been tested extensively on a variety of real cases (e.g., Gong et al. 2003; Liu et al. 2005; Zhang and Wang 2006; Xu et al. 2011). However, even these sophisticated dealiasing algorithms encountered difficulties in certain situations, such as in a strong shear region and multiple-aliased area.

The purpose of this paper is to present the gradient velocity track display (GrVTD) technique specifically for alleviating velocity aliasing in data collected in intense atmospheric vortices (e.g., tropical cyclones, mesocyclones, and tornadoes) by research and operational radars. The GrVTD technique applies the GVAD concept to the GBVTD technique so that the aliased Doppler velocities can be directly used. The same approach can be applied to the entire family of VTD techniques in principle except for the GVTD.[2] Although the gradients of V_d are sensitive to the azimuthal variation of V_d and random errors, the GrVTD and GBVTD will be shown to produce consistent and comparable results in both analytical and real TCs.

This paper is organized as follows. Section 2 describes the mathematical formulations of GrVTD and its characteristics. In section 3, analytic datasets are employed to quantitatively evaluate the sensitivity to aliasing, random errors, tangential wind asymmetry, mean wind, and center estimates. In section 4, the GrVTD is applied to the WSR-88D data in Hurricane Charley (2004) and compared the retrieved winds with those deduced by GBVTD. Summary and discussion are given in section 5.

[2] Gradient implementation of GVTD involves both V_d and its azimuthal gradient. Therefore, Gradient GVTD is not immune to aliased Doppler velocity.

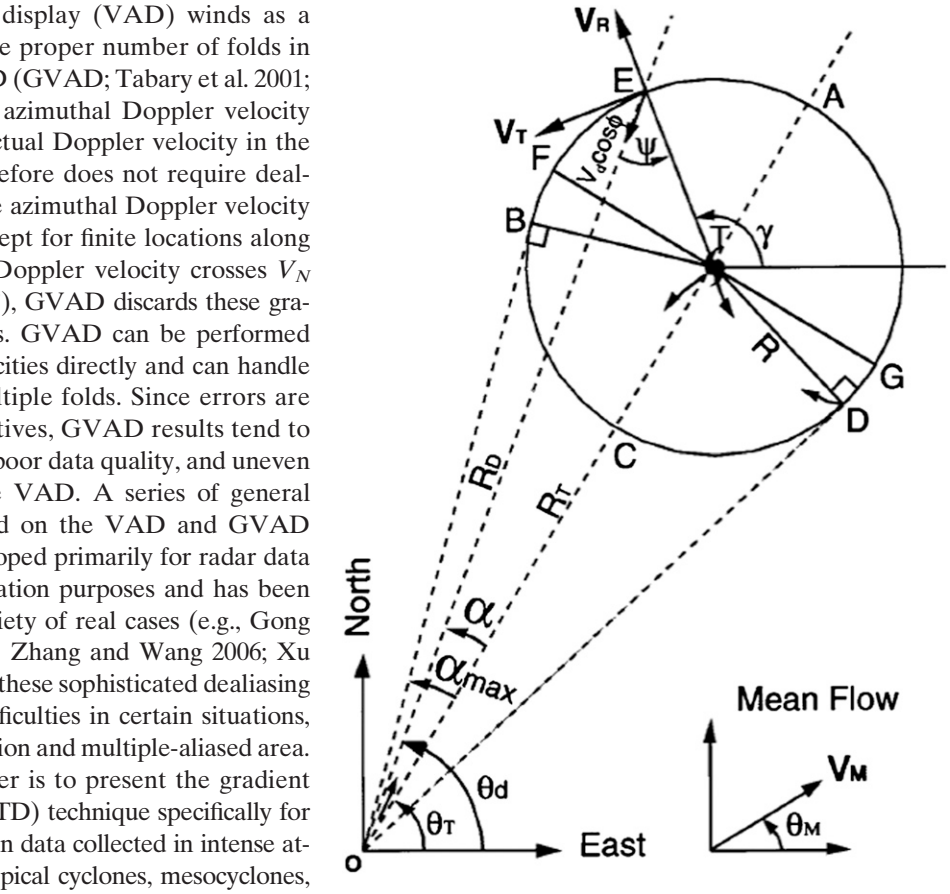

FIG. 1. The geometry and symbols used in GBVTD (adapted from LJCD).

2. The GrVTD technique

a. Mathematical formulation

Using the same geometrical relationship and symbols as in LJCD (Fig. 1), the horizontal projection of Doppler velocity on a GBVTD ring derived from the tangential wind (V_T), the radial wind (V_R), and the mean wind (V_M) is given by

$$\frac{\hat{V}_d}{\cos\phi} = V_M\left[\cos(\theta_T - \theta_M)\left(\frac{1-\cos\alpha_{\max}}{2}\cos 2\psi + \frac{1+\cos\alpha_{\max}}{2}\right) - \sin(\theta_T - \theta_M)\sin\alpha_{\max}\sin\psi\right] - V_T\sin\psi + V_R\cos\psi, \quad (3)$$

where ϕ is the elevation angle. Note V_M is a function of altitude only. Interested readers can find the definitions of variables in LJCD, their appendix A.

Approximating $\hat{V}_d/\cos\phi$ with V_d as in Jou et al. (2008), the azimuthal gradient of V_d can be obtained by taking

the derivative of (3) with respect to azimuth relative to vortex center (referred to as azimuth):

$$\frac{\partial(V_d)}{\partial\psi} = -V_M\cos(\theta_T - \theta_M)(1 - \cos\alpha_{\max})\sin2\psi - V_M\sin(\theta_T - \theta_M)\sin\alpha_{\max}\cos\psi - V_T\cos\psi - \frac{\partial V_T}{\partial\psi}\sin\psi - V_R\sin\psi + \frac{\partial V_R}{\partial\psi}\cos\psi. \quad (4)$$

Following LJCD, V_d, V_T, and V_R can be expanded into Fourier components in the ψ coordinates

$$V_d = \sum_{n=0}^{N} A_n\cos(n\psi) + \sum_{n=0}^{N} B_n\sin(n\psi), \quad (5)$$

$$V_T = \sum_{m=0}^{M} V_T C_m\cos(m\psi) + \sum_{m=0}^{M} V_T S_m\sin(m\psi), \quad \text{and} \quad (6)$$

$$V_R = \sum_{m=0}^{M} V_R C_m\cos(m\psi) + \sum_{m=0}^{M} V_R S_m\sin(m\psi), \quad (7)$$

where A_n ($V_T C_m$ and $V_R C_m$) and B_n ($V_T S_m$ and $V_R S_m$) are the coefficients of the sine and cosine components of V_d (V_T and V_R), respectively, for the azimuthal wavenumber n (m) and typically $N = M + 1$.

From (5), the derivative of V_d on ψ can be written as

$$\frac{\partial V_d}{\partial\psi} = -\sum_{n=1}^{N} nA_n\sin n\psi + \sum_{n=1}^{N} nB_n\cos n\psi. \quad (8)$$

The Fourier coefficients A_n and B_n can be obtained, and V_T and V_R from wavenumbers 0 to 3 can be solved from (4), (6), and (7) as follows:

$$V_T C_0 = -B_1 - B_3 - V_M\sin(\theta_T - \theta_M)\sin\alpha_{\max} + V_R S_2, \quad (9)$$

$$V_R C_0 = A_1 + A_3 - V_R C_2, \quad (10)$$

$$V_T C_1 = -2(B_2 + B_4) + V_R S_1 + 2V_R S_3, \quad (11)$$

$$V_T S_1 = 2(A_2 + A_4) - V_R C_1 - 2V_R C_3 - V_M\cos(\theta_T - \theta_M)(1 - \cos\alpha_{\max}), \quad (12)$$

$$V_T C_2 = -2B_3 + V_R S_2, \quad (13)$$

$$V_T S_2 = 2A_3 - V_R C_2, \quad (14)$$

$$V_T C_3 = -2B_4 + V_R S_3, \quad \text{and} \quad (15)$$

$$V_T S_3 = 2A_4 - V_R C_3, \quad (16)$$

where $V_M\cos(\theta_T - \theta_M)$ (referred to as $V_{M\|}$) and $V_M\sin(\theta_T - \theta_M)$ (referred to as $V_{M\perp}$) represent the along-beam and cross-beam components of the mean wind in the direction of the radar beam passing through the TC center, respectively. By substituting (2) into (8), the gradients of V_d and V_u are equivalent as the derivative of $2nV_N$ with respect to azimuth equals to zero except in the boundary between aliased and nonaliased area. Thus, the advantage of this method is that it cannot be influenced by velocity aliasing. However, as shown in (8), the constant term A_0 vanishes by taking derivative of ψ. As a result, $V_{M\|}$ is not resolved and it is aliased into the wavenumber 1 component of the tangential wind $V_T S_1$ in (12), which has a slightly different form as compared to LJCD, their Eq. (22). In addition, GrVTD faces similar limitations to those encountered in GBVTD where the number of unknown variables is greater than the number of equations. Hence, the same closure assumptions are used as in GBVTD; namely, the asymmetric V_R is smaller than axisymmetric V_R and therefore can be ignored. As pointed out by LCJD, the maximum wavenumber resolved at each radius varies with the maximum angular data gap; for data having gaps of 30°, 60°, 120°, and 180°, the maximum wavenumbers resolved are 3, 2, 1, and 0, respectively.

b. Compute gradients of V_d

In the GVAD technique, the Fourier analysis is performed directly on the circle of a radar scan; thus, the extra step of interpolation is not necessary. The azimuthal gradients of V_d can be calculated simply by taking the difference of V_d at adjacent points in the azimuthal direction. To minimize the impact of velocity ambiguity and random errors, Gao et al. (2004) eliminate the abnormally large $\partial V_d/\partial\psi$ at the folding points, and then apply a simple low-pass filter to reduce random noise [see their Eqs. (11) and (12)].

In contrast, the GrVTD is performed on a cylindrical coordinate system centered at the TC, so it requires the radar data first be interpolated from the radar-centered spherical coordinate system to the TC-centered cylindrical coordinates. In this study, V_d in each PPI is interpolated onto CAPPI first, and then is bilinearly interpolated onto an evenly spaced azimuthal grid (at 1° intervals) at a constant radius from the TC center (on ψ coordinate), as illustrated in LJCD. The horizontal bilinear interpolation uses four V_d observations (defined as V_i, $i = 1, \ldots, 4$) from two adjacent beams in azimuth and two gates in range surrounding each destination grid point in space. To eliminate the impact of aliasing during the interpolation surrounding those folding points, a local dealiasing method (Miller et al. 1986) is employed.

Taking any one of these four measured values (V_e) as a reference, the remaining three values are forced into the ambiguous velocity interval centered on this reference value using (2). The proper Nyquist number (n) is calculated as follows:

$$n = \begin{cases} \text{INT}(K + 0.5), & \text{if} \quad \text{K} \geq 0 \\ \text{INT}(K - 0.5), & \text{if} \quad K < 0 \end{cases}$$
$$K = \frac{V_i - V_e}{2V_N}, \quad i = 1, \ldots, 4 \quad V_i \neq V_e, \qquad (17)$$

where INT represents truncation toward zero, and K represents the appropriate unfolding factor.

The vertical bilinear interpolation between two successive elevations to a CAPPI can be performed the same way to ensure all V_ds affecting a grid point are in the same Nyquist interval. When the Nyquist velocity changes between successive elevations (e.g., with VCP 21 of WSR-88D radars), the vertical nearest-neighbor mapping is performed instead of interpolation. A similar local dealiasing is performed when interpolating data from CAPPI to TC cylindrical coordinate (ψ). Once the V_ds on the GBVTD ring are obtained, the azimuthal gradient of V_d with respect to ψ can be calculated by taking the difference of V_d at adjacent points in the azimuthal direction with a constant azimuth interval (a 1° interval is used here). To avoid the discontinuity of $\partial V_d/\partial\psi$ occurring at the folding points as in Gao et al. (2004), a similar local dealiasing is also applied to the calculation of the gradients using

$$\left(\frac{\partial V_d}{\partial \psi}\right)^j = \frac{(V_d^{j+1} - V_d^{j-1}) + 2nV_N}{\psi^{j+1} - \psi^{j-1}}$$
$$n = \text{INT}[(V_d^{j-1} - V_d^{j+1})/V_N]. \qquad (18)$$

Here j is the index of the data point on the GBVTD ring at a given height and radius.

Next, a quality control procedure is performed to eliminate some outliers in the gradients, and the same low-pass filter as in Gao et al. (2004) is applied to reduce random noise. After applying this filter, the gradients are smoothed and hold their integrity when V_d observations are relatively dense. When the GrVTD method is applied to observations whose coverage is sparse, the total number of valid gradients may be distinctly fewer than the total number of original data, and then GrVTD may fail in a similar manner to the GVAD. Special attentions should be paid to datasets containing unevenly distributed observations and/or large data gaps.

3. Tests using analytic data

a. Construction of the analytic dataset

To quantitatively evaluate the performance of the GrVTD technique, a set of idealized vortex flow fields, which are based on a single-level, idealized Rankine combined vortex, is constructed to simulate the Doppler velocity, V_d, following LJCD. The mathematical expressions for the axisymmetric V_T and V_R are

$$V_T = V_{\max}\frac{R}{R_{\max}}, \quad R \leq R_{\max}$$
$$V_T = V_{\max}\frac{R_{\max}}{R}, \quad R > R_{\max} \qquad (19)$$

$$V_R = C_1[(R_{\max} - R)R]^{1/2}, \quad R \leq R_{\max}$$
$$V_R = C_2(R - R_{\max})^{1/2}R_{\max}/R, \quad R > R_{\max}, \qquad (20)$$

where $V_{\max}$ and $R_{\max}$ are set to 50 m s^{-1} and 20 km, respectively; C_1 and C_2 are scale factors and are assigned 0.1 s^{-1} and 3 m$^{0.5}$ s^{-1}, respectively. According to (20), the outflow (inflow) is inside (outside) the $R_{\max}$. The asymmetric TC circulations are constructed by superimposing higher wavenumbers onto the basic axisymmetric circulation using the following equations:

$$V_T = V_{\max}\frac{R}{R_{\max}}\{1 + W_n \cos[n(\psi - \psi_0)]\}, \quad R \leq R_{\max}$$
$$V_T = V_{\max}\frac{R_{\max}}{R}\{1 + W_n \cos[n(\psi - \psi_0)]\}, \quad R > R_{\max}, \qquad (21)$$

where W_n is the magnitude of each wavenumber and is set to 0.2. Here n represents the wavenumber (n = 1, 2, and 3), and ψ_0 is the phase parameter. Note that there is no asymmetric radial component assumed in the idealized vortex.

A hypothetical Doppler radar is located at the grid origin (0, 0) and has a maximum range of 150 km. The TC center is set at 80 km north of the radar site at (0, 80). The TC circulation generated from (19)–(21) is projected onto the radial direction of the hypothetical radar. LJCD do not consider the velocity aliasing problem; they employ a high effective Doppler velocity. Here, however, V_N is set to 25 m s^{-1} typical of an S-band radar. Additionally, the impact of random errors on the radar-measured V_d is considered by using the following equation:

$$V_d' = V_d + \alpha\varepsilon(0, 1). \qquad (22)$$

Here α is the error amplitude and ε is a random number having a normal Gaussian distribution with zero mean

TABLE 1. Summary of the sensitivity tests on GBVTD and GrVTD. Four test series were conducted to evaluate the impact of aliasing (AL), random error (WR), the asymmetry (AS), and mean wind (VM), respectively. The prefix GB (Gr) represents results from GBVTD (GrVTD).

Test series	Description	Parameter			GBVTD	GrVTD
		V_N (m s^{-1})	α (m s^{-1})	ψ_0 (°)		
AL0	Wave 0 without aliasing	0	0	—	GBAL0	GrAL0
AL1	Wave 0 with aliasing	25	0	—	GBAL1	GrAL1
WR1	Wave 0 + random error	25	1	—	—	GrWR1
WR2	—	25	2	—	—	GrWR2
AS1	Wave 0 + 1	25	1	180	GBAS1	GrAS1
AS2	Wave 0 + 2	25	1	0	GBAS2	GrAS2
AS3	Wave 0 + 3	25	1	90	GBAS3	GrAS3
VM	Wave 0 + mean wind	$V_M = 10$ m s^{-1}, $\theta_T - \theta_M = 0$			—	GrVM

and unity standard deviation. An error standard deviation of 1 m s^{-1} is used for α to represent the standard accuracy of observed V_d for the WSR-88D radar, while a larger error of $\alpha = 2$ m s^{-1} is used for the extreme cases.

The analytic V_d field is used to retrieve the primary circulation of TCs using GBVTD and GrVTD techniques for comparison against the analytic truth. To quantitatively measure the accuracy of GrVTD and GBVTD, the root-mean-square error (RMSE) and relative error (RRE) between retrieved values and analytic values of the tangential winds are calculated as follows:

$$\text{RMSE} = \sqrt{\frac{\sum_{i=1}^{N} (V - V_{\text{ref}})_i^2}{N}} \quad \text{and} \tag{23}$$

$$\text{RRE} = \sqrt{\frac{\sum_{i=1}^{N} (V - V_{\text{ref}})_i^2}{\sum_{i=1}^{N} (V_{\text{ref}})_i^2}}. \tag{24}$$

Here V and V_{ref} are the quantities to be validated and the reference value, respectively; N indicates the total number of valid data points. In addition, the correlation coefficient (CC) between the retrieved and analytic value is also calculated for each experiment.

b. Results of retrieved GrVTD and GBVTD winds

A series of experiments was designed to examine the performances of GBVTD- and GrVTD-retrieved wind fields in the presence of 1) aliasing (AL series), 2) random error (WR series), 3) tangential wind asymmetry (AS series), 4) mean wind (VM series), and 5) center finding error. A description of these experiments is given in Table 1, where the prefixes GB and Gr represent results from GBVTD and GrVTD, respectively.

1) SENSITIVITY TO ALIASING WITHOUT RANDOM ERROR (AL SERIES)

To examine the impact of velocity aliasing on GBVTD and GrVTD methods, two experiments, named AL0 and AL1, are conducted. The V_d data for both experiments are generated from the same analytic axisymmetric vortex with $V_{\max} = 50$ m s^{-1}, $R_{\max} = 20$ km, and $\alpha = 0$ using (19)–(20). AL0 uses V_u (Fig. 2a), while AL1, with a Nyquist velocity of 25 m s^{-1}, uses aliased V_d. The velocity aliasing is particularly noticeable close to the RMW of the vortex (Fig. 2c). The corresponding azimuth profiles of V_u and $\partial V_u/\partial\psi$, and V_d and $\partial V_d/\partial\psi$, at $R = 20$ km and 35 km for AL0 and AL1 are shown in Fig. 2b and Fig. 2d, respectively. Clearly, V_u and $\partial V_u/\partial\psi$ in AL0 are continuous sine or cosine curves with identical amplitudes and phases offset by 90°. In comparison, the aliased V_d in AL1 (solid lines) becomes discontinuous between azimuth 30 (45), 150 (110), 210 (225), and 330 (290) at $R = 20$ km (35 km), while $\partial V_d/\partial\psi$ (dashed lines) still remains the continuous cosine curve with the same shape and magnitude as in AL0. To further examine the impact of multifolding on $\partial V_d/\partial\psi$, the resulting V_d with a V_N of 12.5 m s^{-1} and the azimuth profiles of $\partial V_d/\partial\psi$ are also illustrated in Figs. 2e,f. The curve of $\partial V_d/\partial\psi$ is again nearly identical to that of $\partial V_u/\partial\psi$ in AL0, indicating $\partial V_d/\partial\psi$ is independent of the Nyquist folding number. These results demonstrate that the derived $\partial V_d/\partial\psi$ from (18) is not affected by velocity aliasing, and it might be suitable for directly retrieving the primary circulation of a TC vortex.

The GBVTD- and GrVTD-retrieved tangential wind fields for AL0 and AL1 are illustrated in Figs. 3b–d, as compared with the analytic wind field in Fig. 3a. The GBVTD- (Fig. 3b) and GrVTD- (Fig. 3c) retrieved tangential winds from V_u data both agree well with the analytic wind field (Fig. 3a). The quantitative error statistics of retrieved tangential wind and radial wind for both methods (AL0 in Table 2) also show a consistently

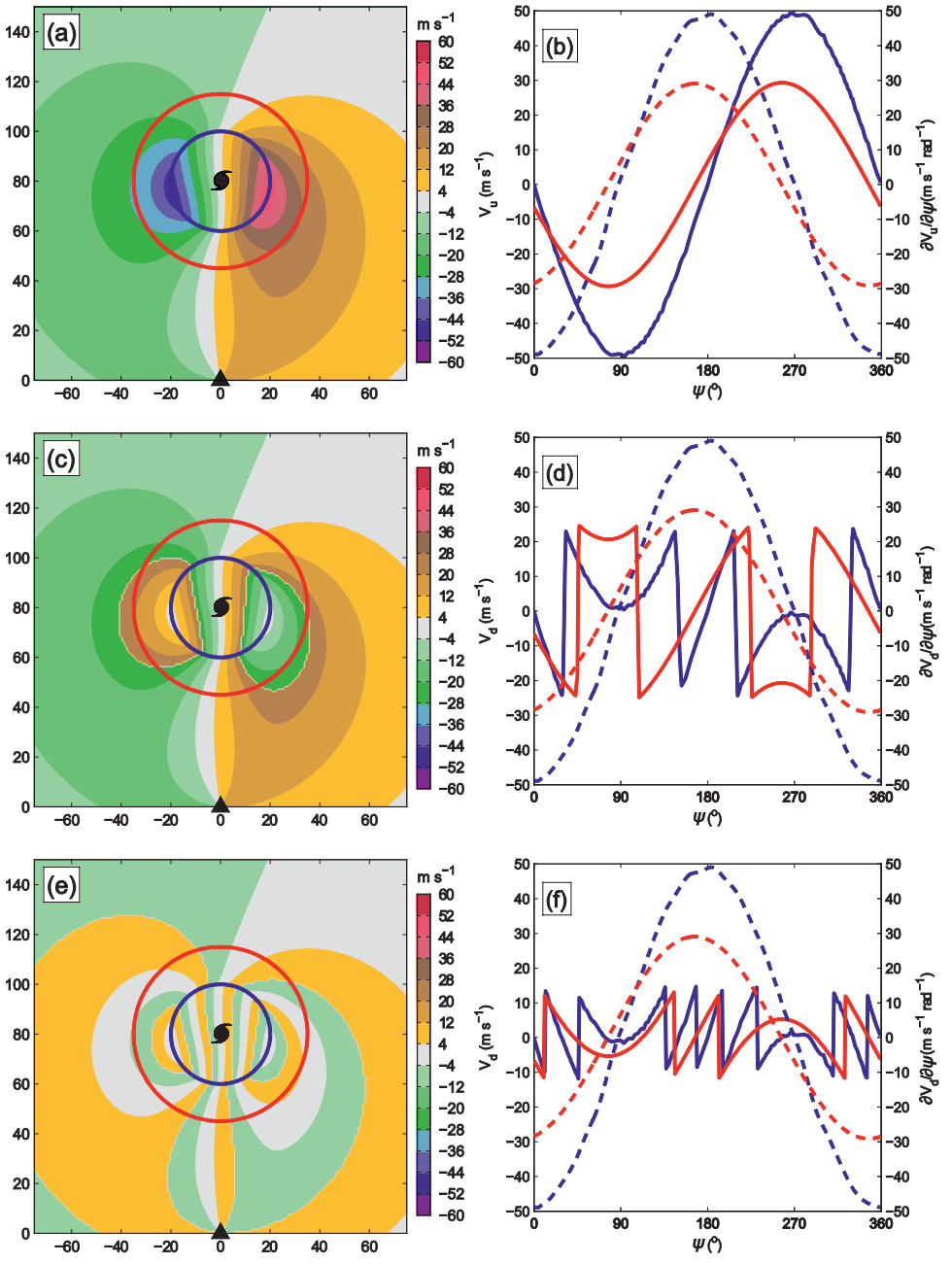

FIG. 2. A comparison of V_d (V_u) and $\partial V_d/\partial\psi$ ($\partial V_u/\partial\psi$) at different radii (noted as blue and red lines) for radial velocities of an axisymmetric vortex with and without aliasing: (a) V_u display and (b) the corresponding V_u (solid line) and $\partial V_u/\partial\psi$ (dashed line) profiles at $R = 20$ (blue curve) and 35 km (red curve); similar to (a),(c),(e) V_d displays with aliasing with Nyquist velocity of 25 and 12 m s^{-1}; and (d),(f) as in (b) but with aliasing.

small RMSE (<0.5 m s^{-1}) and RRE (<5%) and a high CC (close to 1), suggesting that the GrVTD and GBVTD have comparable precision in the case without velocity aliasing. In contrast, the GBVTD-retrieved wind fields (not shown) from V_d show an incorrectly retrieved structure in the inner core of the vortex where the velocity aliasing exists, with the RMSE (RRE) of the tangential wind increasing to 28.1 m s^{-1} (97%) (AL1 in Table 2). The GrVTD, however, can recover the wind pattern (Fig. 3d) well in both structure and magnitude, with its RMSE (RRE) of the tangential wind being about 0.2 (0.6%). These results suggest that GrVTD is able to retrieve the primary circulation of a vortex directly and accurately from V_d data.

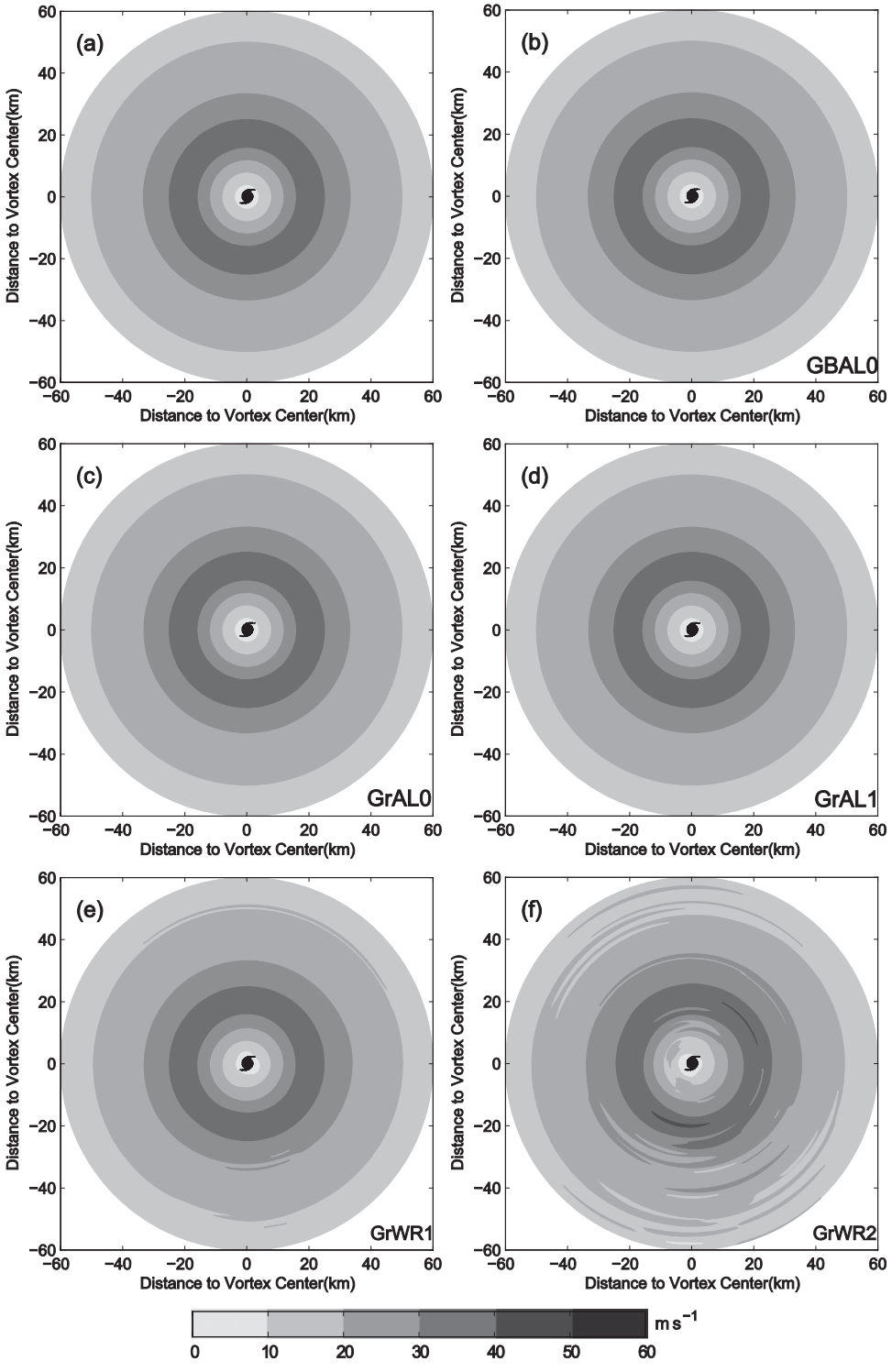

FIG. 3. Comparison between (a) analytic tangential wind and tangential winds retrieved for experiments (b) GBAL0, (c) GrAL0, (d) GrAL1, (e) GrWR1, and (f) GrWR2.

TABLE 2. Sensitivity of GBVTD- and GrVTD-retrieved tangential winds (V_T) and radial winds (V_R) to aliasing.

		Methods			
		GBVTD		GrVTD	
Tests		V_T	V_R	V_T	V_R
AL0	RMS (m s^{-1})	0.1	0.1	0.2	0.3
	RRE (%)	0.4	2	0.6	5
	CC	1.0	1.0	1.0	1.0
AL1	RMS (m s^{-1})	28.1	2.6	0.2	0.3
	RRE (%)	97	51	0.6	5
	CC	−0.67	0.87	1.0	1.0

TABLE 3. Sensitivity of GrVTD-retrieved tangential winds (V_T) and radial winds (V_R) to random errors in radial velocities.

	WR1		WR2	
Errors	V_T	V_R	V_T	V_R
RMSE (m s^{-1})	0.7	0.4	2.0	1.9
RRE (%)	2	9	8	36
CC	1.0	0.99	0.98	0.88

2) SENSITIVITY TO RANDOM ERROR (WR SERIES)

It is well known that V_d usually contains random errors owing to fluctuations of velocity within the sampling volume, range folding, side lobes, etc. (Doviak et al. 1976). To evaluate the impact of random errors, an experiment series WR is conducted in which V_d data contains both velocity aliasing and random errors. The wind field retrieved from the GrVTD with 1 m s^{-1} random error in V_d (WR1) (Fig. 3e) shows good agreement with the analytic wind field (Fig. 3a), except for some small noises. With the random error amplitude increasing to 2 m s^{-1} (WR2), the primary wind structure can still be well captured by GrVTD (Fig. 3f), but the retrieved tangential winds contain more artificial asymmetry signals.

Consistent with the subjective analysis, the quantitative evaluation results also show that the RMSEs of retrieved tangential (radial) winds increase from 0.2 (0.3) m s^{-1} (AL1 in Table 2) to 2.0 (1.9) m s^{-1} (WR2 in Table 3) with the increase of the random error standard deviation from 0 to 2 m s^{-1}. This result is also consistent with increased sensitivity of $\partial V_d/\partial\psi$ to the random error relative to that of V_d (Gao et al. 2004). Considering that the wind speeds in TCs of categories 1–5 are usually greater than 30 m s^{-1}, the RREs of 2–3 m s^{-1} in WR2 are less than 10% of the maximum wind speed. We therefore believe that the accuracy of GrVTD is acceptable. For the 1 m s^{-1} random errors (WR1), the RMSEs for the tangential and radial winds are between those from AL0 and WR2, with values of about 0.7 m s^{-1} and 0.4 m s^{-1}. The RRE of GrVTD-retrieved radial wind is about 9%, greater than that of the tangential wind (2%), because the tangential wind component is much larger than the radial wind component for the idealized vortex.

3) SENSITIVITY TO ASYMMETRY (AS SERIES)

Three experiments are conducted to examine the impact of asymmetric circulation, including wavenumbers 1, 2, and 3 (AS1, AS2, and AS3) embedded within the axisymmetric vortex. The asymmetric structures are generated using (21), and the parameters are listed in Table 1.

Figure 4 shows the analytic (first column) and GrVTD-retrieved (third column) tangential wind fields for wavenumber 1 (first row), 2 (second row), and 3 asymmetries (third row) as compared with GBVTD retrievals using V_u (second column). Similar to that in AL1, GrVTD (Figs. 4c1–c3) can reproduce all major characteristics of wavenumber 1 through 3 structures well, although the retrieved wind fields contain some small noise features. The retrieved asymmetric winds from GrVTD exhibit pronounced distortions for the higher wavenumber asymmetry as shown in the GBVTD analysis from V_u (Figs. 4b1–b3). These distortions can be primarily attributed to the geometric distortion inherent in nonlinear coordinate systems (ψ), which is consistent with the study of LJCD. The corresponding error statistics (Table 4) show that all experiments with asymmetric wind components have a slightly larger error than WR1, which includes only the axisymmetric wind component. The RMSEs (RREs) of the tangential winds for wavenumber 1 through 3 experiments are 0.7 m s^{-1} (3%), 1.1 m s^{-1} (4%), and 3.4 m s^{-1} (12%), respectively, which are close to those from GBVTD using V_u data (not shown). Hence, the GrVTD analysis is also quite robust for asymmetric wind structure retrievals when Doppler velocities are aliased.

4) SENSITIVITY TO MEAN WIND (VM SERIES)

In addition to the limitation shared with GBVTD where $V_{M\perp}$ cannot be resolved, GrVTD cannot resolve $V_{M\parallel}$ either because of the absence of A_0. As shown in (9) and (12), $V_{M\perp}$ and $V_{M\parallel}$ are aliased into the retrieved axisymmetric tangential wind and the wavenumber 1 tangential wind, respectively. As GBVTD and GrVTD have the same equation of axisymmetric tangential wind, their errors in retrieved axisymmetric winds due to the absence of $V_{M\perp}$ are nearly identical and are proportional to the magnitude of $V_{M\perp}$ and the distance from the TC center (see LJCD, their Fig. 11). To quantitatively evaluate the impact of $V_{M\parallel}$ on wavenumber 1 V_T, an experiment VM is conducted by overlapping 10 m s^{-1} $V_{M\parallel}$ (northerly) to the axisymmetric vortex of AL1. The error distribution of wavenumber 1 V_T

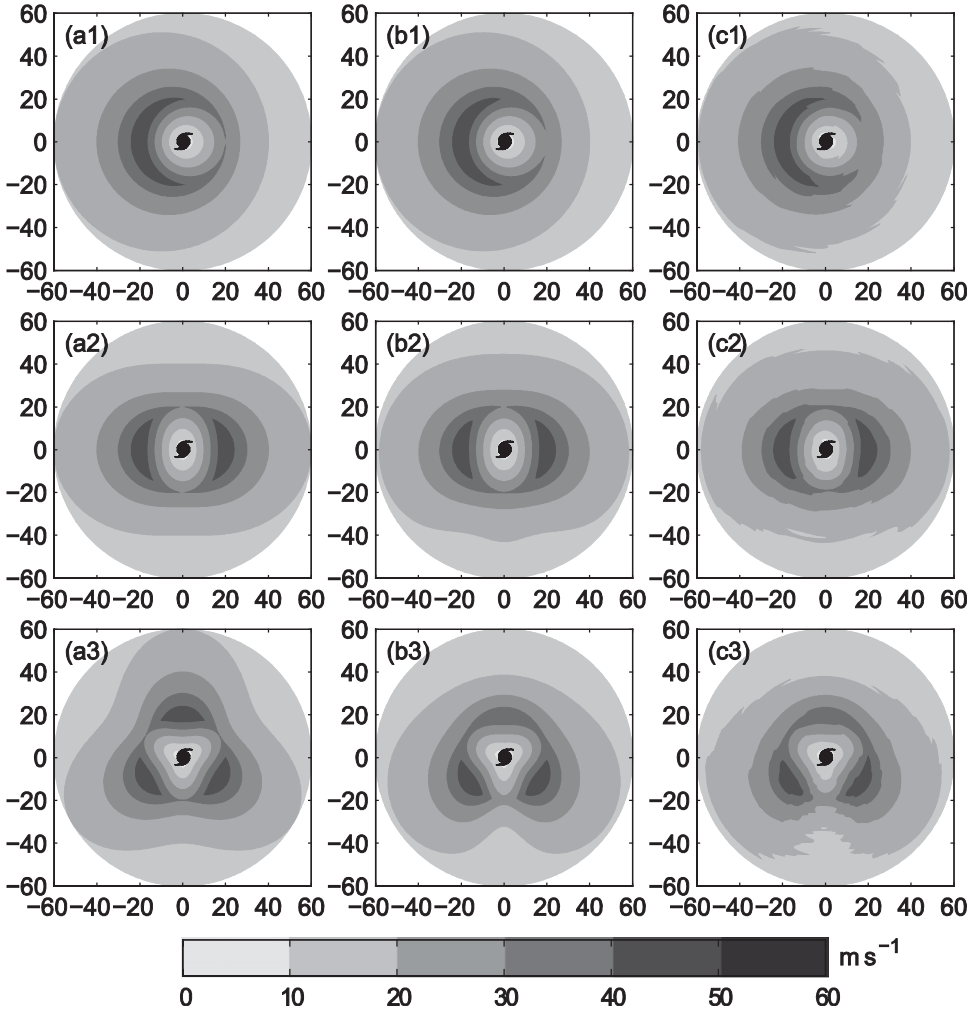

FIG. 4. The (left) analytic tangential wind and (right) GrVTD-retrieved tangential winds for experiment series (top) AS1, (middle) AS2, and (bottom) AS3, as compared to the (center) GBVTD retrievals from V_u. The vortex center is located at (0, 0), while the hypothetical Doppler radar is located at (0, −80).

retrieved by GrVTD is plotted in Fig. 5. The error in the retrieved wavenumber 1 is a sine function of the azimuth angle ψ at each radius from the TC center, with the maximum located at azimuth 90° and 270°. Error also increases with the distance from the TC center, with the maximum increasing from 0.01 m s^{-1} at R = 1 km to about 3 m s^{-1} (~30% of $V_{M\|}$) at 60 km. Such a dependence of the GrVTD-retrieved wavenumber 1 V_T on the distance can be easily interpreted from (12) where the contribution of $V_{M\|}$ is proportional to $(1 - \cos\alpha_{\max})$ that is a function of the distance. If 1 m s^{-1} is the maximum error that can be accepted for the GrVTD-retrieved wavenumber 1 V_T, the upper bound of $(1 - \cos\alpha_{\max})$ should be set to 0.1 ($\sin\alpha_{\max} < 0.43$). For real cases, the upper bound of $(1 - \cos\alpha_{\max})$ can be increased when $V_{M\|}$ is small. It is worth noting that in the analytic experiments here, we have assumed the most severe condition where the retrieved mean wind is set to 0. In fact, methods to estimate the mean wind have been developed in recent years [e.g., the hurricane volume velocity processing method (HVVP; Harasti 2003); the subjective estimation of the mean wind from GVTD (Jou et al. 2008); and using the storm motion as a proxy of mean wind (Harasti et al. 2004)] that have been shown to perform reasonably well in real TC cases. Therefore, there is potential to reduce the wind

TABLE 4. Sensitivity of GrVTD-retrieved tangential winds to tangential wind asymmetry.

Errors	AS1	AS2	AS3
RMSE (m s^{-1})	0.7	1.1	3.4
RRE (%)	3	4	12
CC	1.0	1.0	0.96

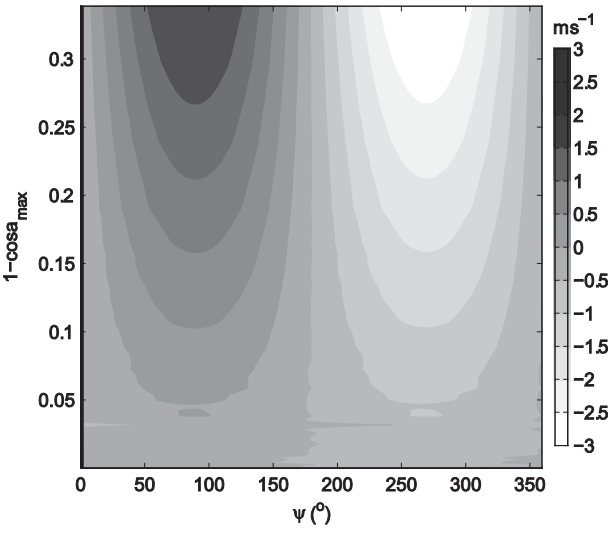

FIG. 5. Error distribution of GrVTD-retrieved wavenumber 1 V_T for experiment GrVM.

retrieval error of GrVTD if the mean wind is estimated using one of these methods.

5) THE GRVTD-SIMPLEX CENTER FINDING

Previous studies (Roux and Marks 1996; Lee and Marks 2000) have shown that the quality of the GBVTD-retrieved winds critically depends on accurately knowing the circulation center. Since GrVTD is based on the same geometric relations as GBVTD, its performance also depends on the accuracy of TC center position. The analytical experiments above retrieve the winds using the true center of the analytical TC. In practice, how to objectively determine a TC circulation center from V_d becomes an important issue for GrVTD. Lee and Marks (2000) combined the "simplex" method (Nelder and Mead 1965) and the GBVTD-retrieved tangential circulations to form an elaborate center finding algorithm, named "GBVTD-simplex," that can identify the TC center with reasonably good accuracy for both analytical and real TCs. They also noted that the estimated center discrepancy needs to be less than 5% RMW to keep the nominal error of the apparent wavenumber 1 less than 20%. However, the GBVTD-simplex algorithm does not work with V_d. In this study, the GrVTD-simplex method similar to GBVTD-simplex is developed to objectively identify TC centers by maximizing GrVTD-retrieved axisymmetric tangential wind.

As described in Lee and Marks (2000), the GrVTD-simplex method begins with an initial TC center and RMW estimated from the single-Doppler velocity dipole signature (Wood and Brown 1992). To search for a global maximum of the mean tangential winds, an array of 16 initial guess centers surrounding this initial center is conducted for subsequent GrVTD-simplex algorithm and yields 16 different simplex center estimates for a given radius within a range of likely RMWs. Finally, the mean and standard deviation of all 16 simplex centers for each radius are computed, and outliers farther than one standard deviation away from the preliminary mean center position are discarded. The optimal TC center is the mean center of the remaining centers at the radius that yields the maximum axisymmetric tangential wind, and the accompanying standard deviation is used as a proxy of the TC center uncertainty.

TABLE 5. The center derived from the GrVTD-simplex algorithm for experiments WR1, AS1, AS2, and AS3.

Expt	Estimated center	Error (km)	Axisymmetric V_T (m s^{-1})
WR1	(−0.05, 79.91)	0.10	48.9
AS1	(−0.38, 80.07)	0.39	49.1
AS2	(−0.07, 79.85)	0.17	48.9
AS3	(−0.26, 80.19)	0.32	48.3
Mean		0.25	

To quantitatively evaluate the performance of the GrVTD-simplex algorithm, the V_d data from experiments WR1, AS1, AS2, and AS3 are employed to estimate the vortex centers. The results (Table 5) show that the mean error of estimated centers is 0.25 km from the true center, which is comparable to 0.34 km in Lee and Marks (2000), where the GBVTD-simplex method was applied to the analytical TCs using V_u. In addition, it is noted that there are no significant differences in the errors of the estimated center among axisymmetric and asymmetric vortex. The maximum error is 0.39 km for AS1, which is still well below the 1-km error threshold (5% of the 20-km RMW) for accurate retrieval of TC asymmetry circulations. Therefore, the GrVTD-simplex is quite robust for objectively determining the center of idealized vortices. The GrVTD-simplex method will be further examined and its center will be used to retrieve circulations of real TC in the next section.

4. Testing of GrVTD with Hurricane Charley (2004)

In this section, GrVTD is tested with data from Hurricane Charley (2004). Charley moved northward across Cuba toward the Florida peninsula on 13 August and was sampled by the WSR-88D radars of Key West, Florida (KBYX), and Tampa, Florida (KTBW), at a 6-min interval during an 18-h period (0800 UTC 13 August to 0200 UTC 14 August) (Lee and Bell 2007). The volume scan at 1402 UTC on 13 August 2004 is chosen to illustrate the performance of GrVTD.

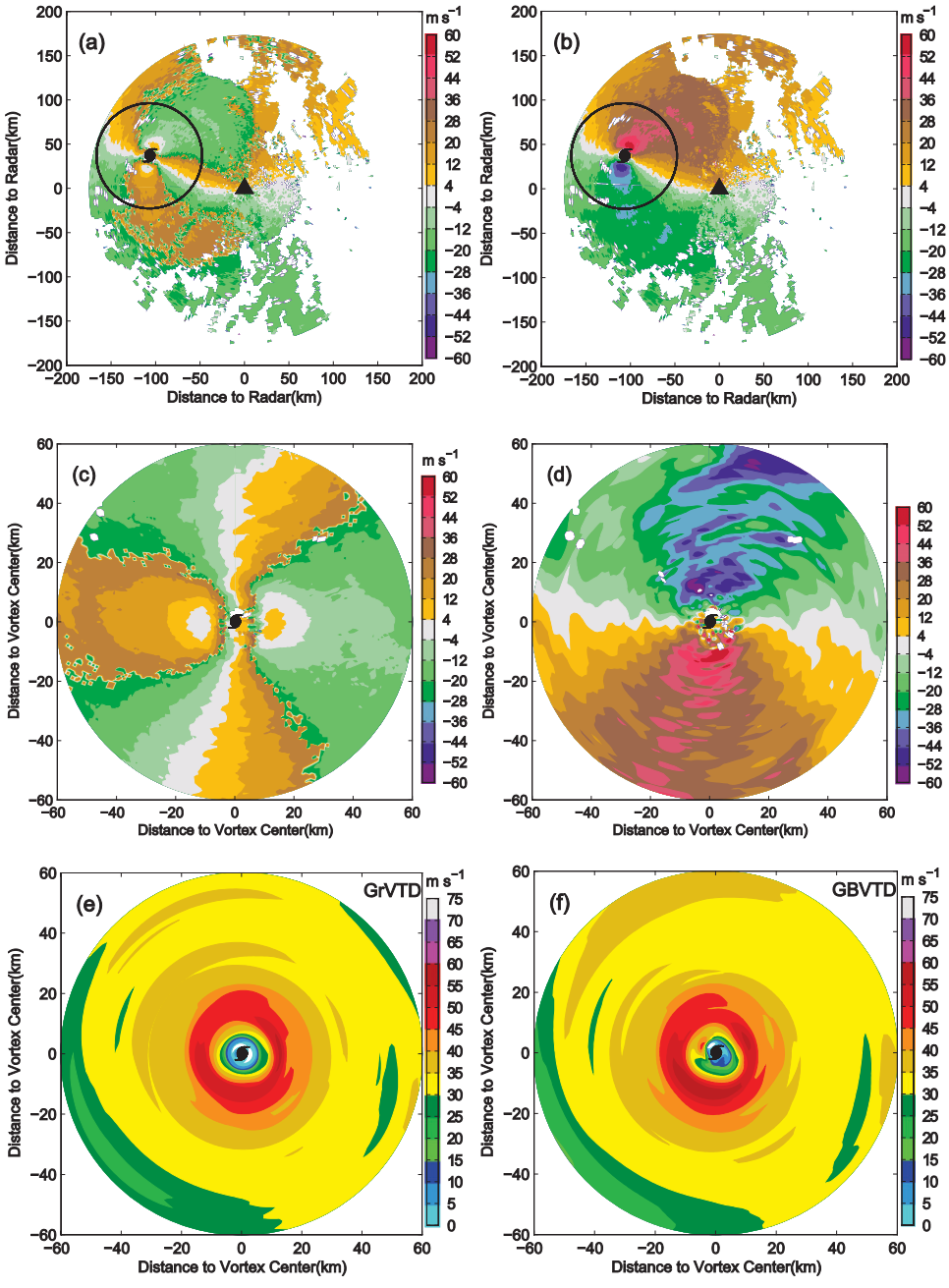

FIG. 6. The (a) raw and (b) dealiased V_d of Hurricane Charley at $Z = 1$ km observed by KBYX on 1402 UTC 13 Aug 2004. The distribution of (c) V_d and (d) its azimuthal gradients (m s^{-1} rad^{-1}) on the GBVTD rings in analysis area [domain enclosed by the black solid circle in (a) and (b)]. The corresponding (e) GrVTD- and (f) GBVTD-retrieved tangential winds derived from (raw, dealiased) radial velocity in the analysis area. The KBYX radar is indicated by a triangle. The hurricane symbol indicates the circulation center of Charley.

The raw radial velocity (V_d) at $Z = 1$ km (Fig. 6a) shows that Charley has a very small eye with an eyewall radius of ~13 km. About half of the V_ds are aliased in Fig. 6a including its inner-core region (indicated by the black circle). The aliasing region can be viewed more clearly in the GBVTD coordinates (Fig. 6c). Figure 6b shows the corresponding dealiased radial velocities (V_u), which were edited and dealiased manually using the National Center for Atmospheric Research (NCAR) interactive ''SOLO'' software. A clear dipole signature emerges in the eyewall through the dealiasing process. Starting from these aliased V_d (Fig. 6c), the

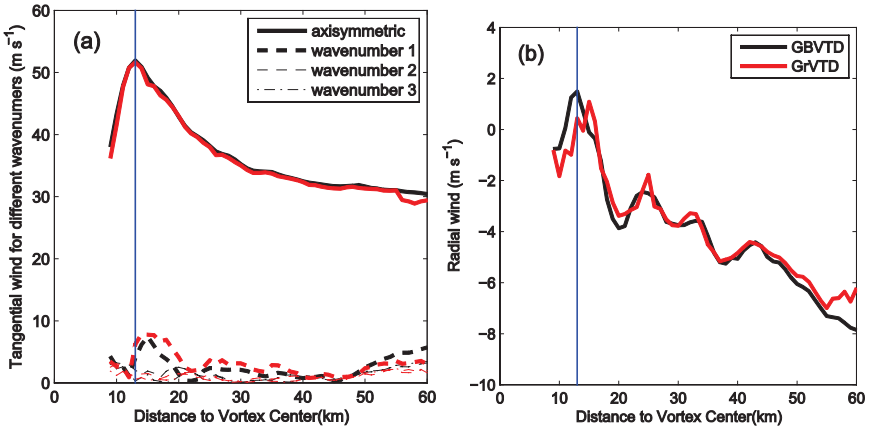

FIG. 7. (a) The amplitudes of wavenumbers 0 to 3 of the tangential wind and (b) the axisymmetric radial wind speed at $Z = 1$ km, retrieved from the GBVTD with dealiased radial velocity (black lines) and GrVTD with aliased radial velocity (red lines). Different line styles represent the different wavenumbers. The vertical blue line indicates the location of the RMW.

GBVTD-retrieved V_T cannot deduce coherent structure as illustrated in the ideal case. Therefore, we will not show those results in this paper. In comparison, using $\partial V_d/\partial\psi$ (Fig. 6d), GrVTD bypasses the effects of aliasing and produces a reasonable retrieval of V_T (Fig. 6e). The retrieved tangential wind shows a distinct wavenumber 1 structure in the eyewall region, with the peak wind located at the southwest quadrant. For comparison, tangential winds are also retrieved from GBVTD using V_u. The GBVTD-retrieved winds from V_u (Fig. 6f) have similar pattern and magnitude as GrVTD retrievals from V_d (Fig. 6e), suggesting the GrVTD is not sensitive to velocity aliasing, which is consistent with those results from analytic experiments. A more careful examination reveals that the major differences between the GrVTD- and GBVTD-retrieved winds are located at $R = 55$ – 60 km in the northwest quadrant and at $R = 15$–20 km south and southwest in the vicinity of eyewall. It is worthwhile to point out that the centers used in GBVTD- and GrVTD-retrieved winds here are estimated from GBVTD- and GrVTD-simplex methods, respectively. Therefore, the center determination discrepancy could be one of reasons for these differences (more on this later). We also applied the GrVTD to other heights. The GrVTD-retrieved winds from V_d are still consistent with the GBVTD retrievals from V_u (not shown).

To further examine the differences between GrVTD with V_d and GBVTD with V_u, the amplitudes of wavenumbers 0 through 3 of the retrieved tangential winds (Fig. 7a) and the axisymmetric radial winds (Fig. 7b) at $Z = 1$ km are analyzed. Overall, both the axisymmetric wind component and asymmetric wavenumber 1 to 3 V_T components from GrVTD and GBVTD are very close, with their mean absolute differences being less than 1 m s^{-1}. The axisymmetric V_Ts from GrVTD and GBVTD are almost identical with the maximum of 52 m s^{-1} at RMW = 13 km. The wavenumber 1 V_T and axisymmetric V_R component have slightly larger differences (about 2 m s^{-1}) between GrVTD and GBVTD, especially within the eyewall ($R < 20$ km) and the outer range (>55 km). These larger differences could be related to the center determination discrepancy, the use of different V_TS_1 expressions in GrVTD [Eq. (12)] and GBVTD [LJCD, their Eq. (22)], and effects of data errors.

To understand how the above factors influence the retrieved winds, we estimate their contributions independently. First, the impact of the difference in the center location is examined by comparing the GrVTD- and GBVTD-retrieved winds that use the GBVTD-simplex center. The centers estimated from GBVTD- and GrVTD-simplex are (−108.40, 36.03) and (−107.65, 36.01), and their difference is about 0.75 km. The corresponding uncertainties of TC centers by the two methods are 0.11 and 0.32 km, both smaller than the 0.65 km (5% RMW) error threshold for accurate retrieval of TC asymmetric circulations. Although the true circulation center is not observed in Charley, the smaller uncertainty of the GBVTD-simplex center suggests a higher confidence level than the GrVTD-simplex center. Using the GBVTD-simplex center, the GrVTD-retrieved wind distribution and magnitude from V_d (Fig. 8a) become closer to the GBVTD-retrieved results. The axisymmetric V_T component (Fig. 8b) is very close to that using the GrVTD-simplex center (Fig. 7a), which is consistent with the fact that the axisymmetric V_T component is less sensitive to the center uncertainty in GBVTD analysis (Lee and Marks 2000). In contrast, the magnitude difference

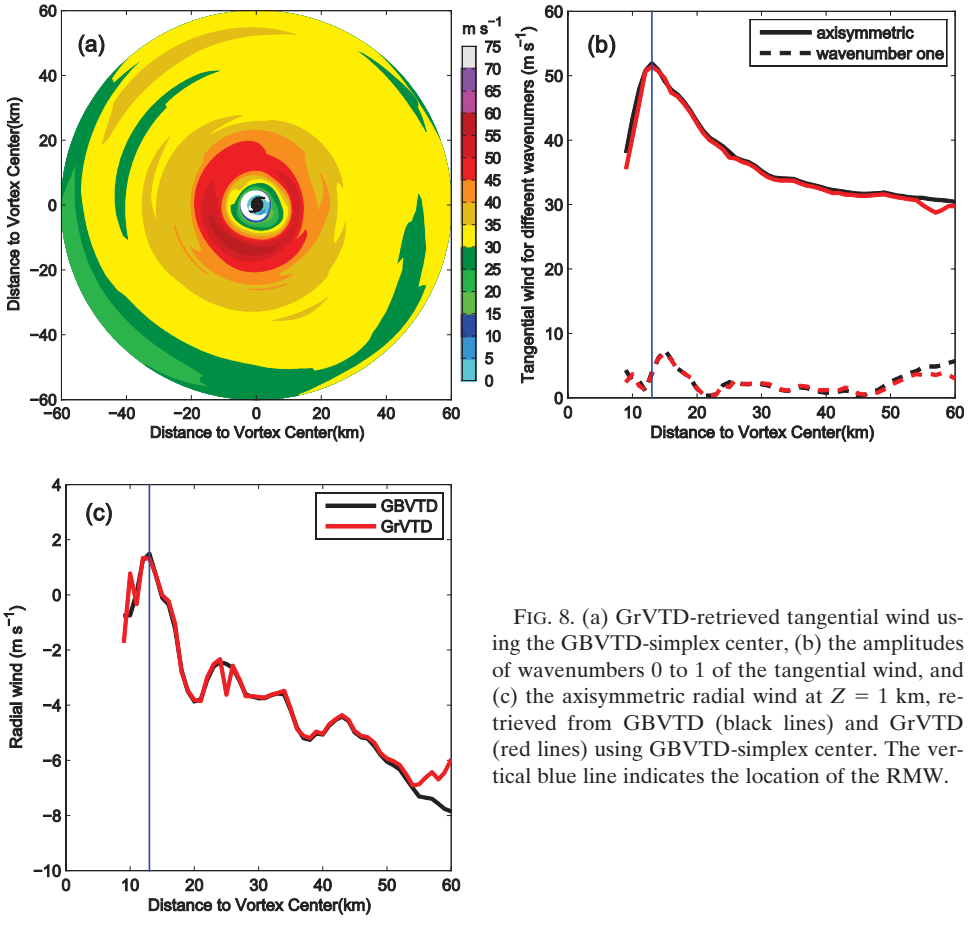

FIG. 8. (a) GrVTD-retrieved tangential wind using the GBVTD-simplex center, (b) the amplitudes of wavenumbers 0 to 1 of the tangential wind, and (c) the axisymmetric radial wind at $Z = 1$ km, retrieved from GBVTD (black lines) and GrVTD (red lines) using GBVTD-simplex center. The vertical blue line indicates the location of the RMW.

in wavenumber 1 V_T (Fig. 8b) and the axisymmetric V_R (Fig. 8c) between GrVTD and GBVTD decreased to less than 1 m s^{-1} at almost all analysis radii except for $R =$ 57–60 km, suggesting that the center determination difference contributes primarily to the difference in the wavenumber 1 V_T and the axisymmetric V_R. Second, we calculate the wavenumber 1 V_T that is aliased from A_0 by substituting the $V_{M\|}$ component (~5 m s^{-1} estimated by GBVTD using V_u data) into (12). The resulting magnitude aliased into wavenumber 1 V_T due to the missing A_0 is within 1 m s^{-1} at all analysis radii, suggesting that the impact of A_0 is small in this case.

5. Summary and discussion

In this paper, the gradient velocity track display (GrVTD) technique is developed based on the GBVTD (LJCD) and GVAD (Gao et al. 2004) techniques. Similar to GBVTD, the GrVTD technique deduces the TC primary circulations, including axisymmetric tangential and radial winds, and wavenumbers 1, 2, and 3 asymmetry of tangential wind. It does so by performing harmonic analysis on the azimuthal gradient of Doppler radial velocity, $\partial V_d/\partial\psi$, rather than the radial velocity (V_d), in a TC-centered cylindrical coordinate. The main advantage of the GrVTD technique over the GBVTD technique is that it does not require velocity dealiasing as a priori. As the performance of GrVTD depends on the accuracy of TC center position, a GrVTD-simplex algorithm similar to GBVTD-simplex is developed to objectively estimate the TC circulation center by maximizing GrVTD-retrieved mean tangential wind.

Using analytic data, the characteristics of the GrVTD method are examined and compared with the GBVTD method. When tested with a number of axisymmetric and asymmetric analytic TCs, the accuracy of GrVTD-retrieved winds from $\partial V_d/\partial\psi$ is within 2 m s^{-1} in most cases. The largest error can reach 3.4 m s^{-1} when the circulation is dominated by wavenumber 3, and can be attributed to geometry distortion (LJCD). Larger random errors added to the data will also slightly increase the error of GrVTD-retrieved winds, as the gradients of V_d are sensitive to random errors.

Results from Hurricane Charley (2004) show that GrVTD can reproduce Charley's primary circulations well from $\partial V_d/\partial\psi$ without prior dealiasing. The pattern

and magnitude of the retrieved total winds are close to those retrieved from GBVTD using manually dealiased V_u. The magnitudes of the axisymmetric, wavenumber 2 and three tangential winds from GrVTD are within 1 m s^{-1} of those deduced from GBVTD. In comparison, wavenumber 1 V_T and axisymmetric V_R components, however, have relatively larger differences in the eyewall region and at R = 55–60 km from the hurricane center. These differences are mainly due to the difference (~0.75 km) in the TC center positions estimated by the two methods. Although the true circulation center is unknown, the GBVTD-simplex center is believed to have a slightly higher confidence level because of a smaller center uncertainty than the GrVTD-simplex center. Overall, GrVTD using aliased velocity directly has a comparable performance to the original GBVTD using manually dealiased velocity.

Besides the aforementioned advantage, GrVTD inherits all known GBVTD limitations stated in section 2. Additional limitations of the GrVTD technique are noted. First, from (8), it can be seen that the constant term A_0 vanishes. As a result, the $V_{M\|}$ is not resolved and it is aliased into $V_T S_1$ (the wavenumber 1 V_T) in (12). As also shown in (12), the wavenumber 1 V_T error due to the absence of $V_{M\|}$ is proportional to the radius from the vortex center, as the $V_{M\|}$ is amplified by a multiplier, $(1 - \cos\alpha_{\max})$. Second, $\partial V_d/\partial\psi$ is more sensitive to random errors in the observations than V_d itself, which may negatively impact the least squares fit of the GrVTD coefficients. As shown in experiment series WR, the RMSE of GrVTD-retrieved V_T (V_R) is proportional to the random error.

Based on tests using analytic TC vortices and a single hurricane case, the ability for the GrVTD algorithm to accurately retrieve the TC primary circulations from aliased radar radial velocity is promising. Preliminary results applying GrVTD to several other TCs are consistent with the findings here. The application of GrVTD to tornado cases will be reported in future papers. Work along this line is underway. Furthermore, by comparing the GrVTD to the other VTD family of techniques, we note that there are trade-offs between the various formulations that would favor one over another in different scenarios (i.e., enhanced center sensitivity but reduced asymmetric distortion in GVTD; reduced mean wind determination and more potential for noise, but enhanced robustness in aliased conditions for GrVTD). Given the strengths and limitations of VTD family of techniques, it is possible to combine these algorithms to maximize their advantages. Given that velocity aliasing is a norm rather than an exception for most TCs, the GrVTD-retrieved winds can be used as a first guess for dealiasing the radial velocity for subsequent use in GBVTD and GVTD. Finally, the GrVTD algorithm enables the real-time retrieval of primary circulations in landfalling TCs. As demonstrated in Zhao et al. (2012), assimilating GBVTD-retrieved primary circulations can improve the structure and intensity analyses and forecasts of TCs compared to directly assimilating radial velocity. With the benefit of being aliasing proof, GrVTD retrievals can be used in a similar way.

Acknowledgments. This work was primarily supported by the National Fundamental Research 973 Program of China (Grant 2009CB421502), the National Natural Science Foundation of China (Grants 40975011 and 40505004), and the Social Common Wealth Research Program (Grant GYHY201006007). M. Xue was supported by ONR Grants N00014-10-1-0133 and N00014-10-1-0775 and NSF Grants AGS-0802888, OCI-0905040, AGS-0941491, AGS-1046171, and AGS-1046081. The National Thousand Plan support to M. Xue facilitated the collaboration. Internal reviews provided by J. Gao and P. Stauffer greatly improved this manuscript. Dr. Robin Tanamachi helped proofread the paper.

REFERENCES

Bargen, D. W., and R. C. Brown, 1980: Interactive radar velocity unfolding. Preprints, *19th Conf. on Radar Meteorology,* Miami, FL, Amer. Meteor. Soc., 278–283.

Baynton, H. W., 1979: The case for Doppler radars along our hurricane affected coasts. *Bull. Amer. Meteor. Soc.,* **60,** 1014–1023.

Bergen, W. R., and S. C. Albers, 1988: Two- and three-dimensional de-aliasing of Doppler radar velocities. *J. Atmos. Oceanic Technol.,* **5,** 305–319.

Doviak, R. J., and D. S. Zrnic, 2006: *Doppler Radar and Weather Observations*. 2nd ed. Dover Publications, 562 pp.

——, P. S. Ray, R. G. Strauch, and L. J. Miller, 1976: Error estimation in wind fields derived from dual-Doppler radar measurement. *J. Appl. Meteor.,* **15,** 868–878.

Gao, J., and K. K. Droegemeier, 2004: A variational technique for dealiasing Doppler radial velocity data. *J. Appl. Meteor.,* **43,** 934–940.

——, ——, J. Gong, and Q. Xu, 2004: A method for retrieving mean horizontal wind profiles from single-Doppler radar observations contaminated by aliasing. *Mon. Wea. Rev.,* **132,** 1399–1409.

Gong, J., L. Wang, and Q. Xu, 2003: A three-step dealiasing method for Doppler velocity data quality control. *J. Atmos. Oceanic Technol.,* **20,** 1738–1748.

Harasti, P. R., 2003: The hurricane volume velocity processing method. Preprints, *31st Int. Conf. on Radar Meteorology,* Seattle, WA, Amer. Meteor. Soc., 14B.1. [Available online at http://ams.confex.com/ams/32BC31R5C/techprogram/paper_64625.htm.]

——, C. J. McAdie, P. P. Dodge, W.-C. Lee, J. Tuttle, S. T. Murillo, and F. D. Marks, 2004: Real-time implementation of single-Doppler radar analysis methods for tropical cyclones: Algorithm improvements and use with WSR-88D display data. *Wea. Forecasting,* **19,** 219–239.

Hennington, L., 1981: Reducing the effects of Doppler radar ambiguities. *J. Appl. Meteor.,* **20,** 1543–1546.

James, C. N., and R. A. Houze, 2001: A real-time four-dimensional Doppler dealiasing scheme. *J. Atmos. Oceanic Technol.,* **18,** 1674–1683.

Jing, Z. Q., and G. Wiener, 1993: Two-dimensional dealiasing of Doppler velocities. *J. Atmos. Oceanic Technol.,* **10,** 798–808.

Jou, B. J.-D., W. C. Lee, S. P. Liu, and Y. C. Kao, 2008: Generalized VTD retrieval of atmospheric vortex kinematic structure. Part I: Formulation and error analysis. *Mon. Wea. Rev.,* **136,** 995–1012.

Lee, W.-C., and F. D. Marks Jr., 2000: Tropical cyclone kinematic structure retrieved from single-Doppler radar observations. Part II: The GBVTD-simplex center finding algorithm. *Mon. Wea. Rev.,* **128,** 1925–1936.

——, and M. M. Bell, 2007: Rapid intensification, eyewall contraction, and breakdown of Hurricane Charley (2004) near landfall. *Geophys. Res. Lett.,* **34,** L02802, doi:10.1029/2006GL027889.

——, F. D. Marks Jr., and R. E. Carbone, 1994: Velocity track display (VTD)—A technique to extract real-time tropical cyclone circulations using a single airborne Doppler radar. *J. Atmos. Oceanic Technol.,* **11,** 337–356.

——, B. J.-D. Jou, P.-L. Chang, and S.-M. Deng, 1999: Tropical cyclone kinematic structure retrieved from single-Doppler radar observations. Part I: Interpretation of Doppler velocity patterns and the GBVTD technique. *Mon. Wea. Rev.,* **127,** 2419–2439.

——, ——, and F. D. Marks Jr., 2000: Tropical cyclone kinematic structure retrieved from single-Doppler radar observations. Part III: Evolution and structures of Typhoon Alex (1987). *Mon. Wea. Rev.,* **128,** 3982–4001.

Liou, Y.-C., T.-C. C. Wang, W.-C. Lee, and Y.-J. Chang, 2006: The retrieval of asymmetric tropical cyclone structures using Doppler radar simulations and observations with the extended GBVTD technique. *Mon. Wea. Rev.,* **134,** 1140–1160.

Liu, S., Q. Xu, and P. F. Zhang, 2005: Identifying Doppler velocity contamination caused by migrating birds. Part II: Bayes identification and probability tests. *J. Atmos. Oceanic Technol.,* **22,** 1114–1121.

Miller, L. J., C. G. Mohr, and A. J. Weinheime, 1986: The simple rectification to Cartesian space of folded radial velocities from Doppler radar sampling. *J. Atmos. Oceanic Technol.,* **3,** 162–174.

Nelder, J. A., and R. Mead, 1965: A simplex method for function minimization. *Comput. J.,* **7,** 308–313.

Oye, R., C. Mueller, and S. Smith, 1995: Software for radar translation, visualization, editing, and interpolation. Preprints, *27th Conf. on Radar Meteorology,* Vail, CO, Amer. Meteor. Soc., 359–361.

Roux, F., and F. D. Marks, 1996: Extended velocity track display (EVTD): An improved processing method for Doppler radar observations of tropical cyclones. *J. Atmos. Oceanic Technol.,* **13,** 875–899.

——, F. Chane-Ming, A. Lasserre-Bigorry, and O. Nuissier, 2004: Structure and evolution of intense Tropical Cyclone Dina near La Réunion on 22 January 2002: GB-EVTD analysis of single Doppler radar observations. *J. Atmos. Oceanic Technol.,* **21,** 1501–1518.

Tabary, P., G. Scialom, and U. Germann, 2001: Real-time retrieval of the wind from aliased velocities measured by Doppler radars. *J. Atmos. Oceanic Technol.,* **18,** 875–882.

Wood, V. T., and R. A. Brown, 1992: Effects of radar proximity on single-Doppler velocity signatures of axisymmetric rotation and divergence. *Mon. Wea. Rev.,* **120,** 2798–2807.

Xu, Q., K. Nai, L. Wei, P. F. Zhang, S. Liu, and D. Parrish, 2011: A VAD-based dealiasing method for Radar velocity data quality control. *J. Atmos. Oceanic Technol.,* **28,** 50–62.

Yamada, Y., and M. Chong, 1999: Vad-based determination of the Nyquist internal number of Doppler velocity aliasing without wind information. *J. Meteor. Soc. Japan,* **77,** 447–457.

Zhang, J., and S. Wang, 2006: An automated 2D multipass Doppler radar velocity dealiasing scheme. *J. Atmos. Oceanic Technol.,* **23,** 1239–1248.

Zhao, K., W. C. Lee, and B. J.-D. Jou, 2008: Single Doppler radar observation of the concentric eyewall in Typhoon Saomai, 2006, near landfall. *Geophys. Res. Lett.,* **35,** L07807, doi:10.1029/2007GL032773.

——, M. Xue, and W.-C. Lee, 2012: Assimilation of GBVTD-retrieved winds from single-Doppler radar for short-term forecasting of Super Typhoon Saomai (0608) at landfall. *Quart. J. Roy. Meteor. Soc.,* **138,** 1055–1071, doi:10.1002/qj.975.

Zittel, W. D., and T. Wiegman, 2005: VCP 121 and the multi-PRF dealiasing algorithm. *NEXRAD Now,* No. 14, 9–15. [Available online at http://www.roc.noaa.gov/WSR88D/PublicDocs/NNOW/NNwinter05d.pdf.]